

## SUPPORTING INFORMATION

### Copper Peroxide incorporated BSA-NPs: A pH-responsive, self-supplying source of Reactive Oxygen Species for Cancer Cell Destruction via Polarization of Macrophages to M1 Phenotype

Nursaima Sultana Parbin<sup>a, b</sup>, Bhabatosh Banik<sup>\*a</sup>

<sup>a</sup> Department of Chemistry, Cotton University, Panbazar, Guwahati-781001, Assam, India

<sup>b</sup> Department of Chemistry, Gauhati University, Gopinath Bordoloi Nagar, Guwahati-781014, Assam, India

\*To whom correspondence should be addressed

E-mail: [bhabatosh.banik@cottonuniversity.ac.in](mailto:bhabatosh.banik@cottonuniversity.ac.in)

#### Table of contents

1. Experimental Section	
2. Comparison of reported ROS-generating NPs used for polarization of macrophages with CuPer-BSA-NPs (present work)	Table S1
3. Size and zeta potential comparison of the nanoparticles	Table S2
4. Schematic representation of the synthetic approach for CuPer <sub>x</sub> -BSA-NPs	Scheme S1
5. DLS size histograms obtained for BSA-NP and CuPer <sub>x</sub> -BSA-NPs.	Figure S1
6. Representative Calibration curve for Cu Quantification	Figure S2
7. Percentage Loading (% L), Percentage Incorporation Efficiency (% IE) and Cu concentration (in ppm) of CuPer-BSA-NPs	Table S3
8. SEM images for BSA-NP and CuPer-BSA-NP	Figure S3
9. SEM images for control nanoparticle synthesis experiments	Figure S4
10. Energy dispersive X-ray analysis (EDAX) of BSA-NP and CuPer-BSA-NPs	Figure S5
11. Surface composition of the nanoparticles	Table S4
12. Time-dependent stability study for CuPer <sub>25</sub> -BSA-NPs	Figure S6
13. TEM image and EDS mapping analysis of CuPer <sub>25</sub> -BSA-NPs	Figure S7
14. X-ray Photoelectron Spectrum of CuPer <sub>25</sub> -BSA-NPs	Figure S8
15. KMnO <sub>4</sub> decolorization control experiment (pH 7.4 and Cu/H <sub>2</sub> O <sub>2</sub> )	Figure S9
16. Representative images for the solutions in a KMnO <sub>4</sub> decolorization assay	Figure S10
17. Representative images for the solutions of TMB oxidation assay	Figure S11
18. Control TMB oxidation experiments	Figure S12
19. Lineweaver-Burk plot and Absorbance vs. TMB concentration plot for determination of amount of H <sub>2</sub> O <sub>2</sub> concentration	Figure S13
20. TMB oxidation assay in buffer media containing FBS	Figure S14
21. Representative images for the solutions of TMB oxidation assay in 1% FBS-containing buffer	Figure S15
22. Representative images for the solutions of TMB oxidation assay in 10% FBS-containing buffer	Figure S16
23. pH-dependent stability study for CuPer <sub>25</sub> -BSA-NP	Figure S17
24. DCFDA assay on RAW 264.7 cells using 0.5 ppm CuPer <sub>25</sub> -BSA-NPs	Figure S18
25. Fluorescence microscopy images of untreated, BSA-NP treated and CuPer <sub>25</sub> -BSA-NP treated RAW 264.7 cells	Figure S19
26. Scheme of the experiment performed to determine the toxicity of conditioned media	Scheme S2

## EXPERIMENTAL SECTION

**Materials:** All the chemicals and solvents were procured from commercial sources and were used without further purification. Copper chloride ( $\text{CuCl}_2 \cdot 2\text{H}_2\text{O}$ ), Sodium hydroxide (NaOH), Hydrogen peroxide ( $\text{H}_2\text{O}_2$ ), Sodium acetate ( $\text{CH}_3\text{COONa} \cdot 3\text{H}_2\text{O}$ ), Acetic acid ( $\text{CH}_3\text{COOH}$ ), Nitric Acid and Patton and Reeder's (PR) indicator were obtained from Merck. Glutaraldehyde ( $\text{C}_3\text{H}_6\text{O}_3$ ) was purchased from Spectrochem. Bovine Serum Albumin (BSA) was purchased from Himedia. Tetradecyltrimethylammonium chloride (TTAC), Griess reagent (modified), MTT [3-(4,5-dimethylthiazol-2-yl)-2,5-diphenyltetrazolium bromide] and TMB (3,3',5,5'-tetramethylbenzidine) were bought from Sigma-Aldrich. Regenerative cellulose membrane amicon ultracentrifugal 100 kDa filters were purchased from Merck Millipore Ltd. Glutamine, penicillin/streptomycin and sodium pyruvate were purchased from Sigma Life Sciences. Dulbecco's Modified Eagle Medium (DMEM), Fetal Bovine Serum (FBS), HEPES buffer, and sodium pyruvate were purchased from Gibco Life Sciences. Allophycocyanin (APC)-conjugated monoclonal rat primary antibody against murine CD206 and Alexa Fluor 488-conjugated monoclonal rat antibody against murine iNOS were procured from eBioscience™.

**Instrumentations:** FESEM images and EDAX analysis were obtained using a Carl Zeiss scanning electron microscope (Model: Sigma 300 VP). TEM images and EDS mapping analysis were obtained using JEOL Field emission Transmission electron microscope (Model: 2100 F). X-ray photoelectron spectroscopy (XPS) was performed using an X-Ray Photoelectron Spectrometer (XPS) (Thermo Fisher Scientific Pvt. Ltd; UK, ESCALAB Xi+). Dynamic light scattering (DLS) measurements were performed to determine the zeta potential ( $\xi$ )- and particle size of the system using Malvern NanoZS90 and a NICOMP zeta sizer instrument. Electronic transitions of the samples in aqueous media were recorded at room temperature using a UV-1800 Shimadzu Spectrophotometer. MTT assay data were recorded using a Spectra Max iD5 multi-mode microplate reader instrument. Fluorescence microscopy images were acquired using a Zeiss ApoTome inverted fluorescence microscope.

### Methods:

**1. Cell Line and Cell Culture.** Mouse macrophage RAW 264.7 cells were procured from National Centre for Cell Science (NCCS), Pune. RAW 264.7 cells were grown in Roswell Park Memorial Institute (RPMI) medium supplemented with Fetal bovine serum (FBS), L-glutamine, HEPES buffer, and sodium pyruvate at 37 °C in 5%  $\text{CO}_2$ .

**2.Synthesis of CuPer<sub>x</sub>-BSA-NPs:** BSA (10 mg) was dissolved in de-ionized water in a round bottom flask. Volume of de-ionized water used to dissolve BSA was chosen so as to maintain the total volume of reaction mixture at 1900  $\mu\text{L}$  post the addition of  $\text{CuCl}_2 \cdot 2\text{H}_2\text{O}$  solution. Various volumes (250  $\mu\text{L}$ , 500  $\mu\text{L}$ , 750  $\mu\text{L}$  and 1000  $\mu\text{L}$  for  $x= 12.5, 25, 50$  and  $75$  respectively) of aqueous  $\text{CuCl}_2 \cdot 2\text{H}_2\text{O}$  solution (100 mM), was added to the above BSA solution in a dropwise manner under constant stirring. Subscript 'x' in the nomenclature of the NPs denotes the feed of  $\text{CuCl}_2 \cdot 2\text{H}_2\text{O}$  in mM. Then, an aqueous solution of NaOH (0.05 mL, 20 mM) and  $\text{H}_2\text{O}_2$  (0.05 mL, 30%) were also added sequentially to the above mixture. On addition of  $\text{H}_2\text{O}_2$  the bluish color of the reaction mixture turns pale. After 30 minutes of stirring at room temperature an aqueous solution of glutaraldehyde (0.02 mL, 8%) was added. After 24 h of stirring at room temperature the CuPer<sub>x</sub>-BSA-NPs were purified by centrifugal filtration through 100,000 MWCO Amicon filters and washed 3X with de-ionized water. The resultant NP solution was re-suspended in 2 mL de-ionized water and stored at 4 °C.

**3.Synthesis of BSA-NP:** BSA (10 mg) was dissolved in 2 mL de-ionized water in a round bottom flask. Aqueous NaOH solution (0.1 M) was then added to adjust the pH ~8 of the reaction mixture and was allowed to stir for 30 minutes at room temperature. Absolute ethanol (4 mL) was added very slowly in a drop wise manner to the above mixture and stirred for another 30 minutes. Glutaraldehyde solution (0.04 mL, 8%) was finally added to the reaction mixture. After 24 hrs of stirring at room temperature BSA-NPs were purified by Amicon filtration and washed 3X with de-ionized water. The resultant NP solution was re-suspended in 2 mL de-ionized water and stored at 4 °C.

**4.DLS measurement:** To determine the size and zeta potential of the NPs, Dynamic light scattering (DLS) Measurements were performed. For this we have taken 400  $\mu\text{L}$  of nanoparticles in an insert and subjected it to DLS measurements by using NICOMP zeta sizer instrument.

**5.SEM & EDAX analysis:** Surface morphology of the synthesized nanoparticles was determined using Scanning Electron Microscope (SEM) and the surface elemental composition of the nanoparticles was determined using Energy dispersive X-ray (EDAX) Analysis. For this we have diluted the stock nanoparticles by 100X in diluted water and drop casted it on silicon wafer surface. The sample was dried under vacuum and subjected to SEM & EDAX analysis.

**6. FETEM and EDS mapping analysis:** To examine the shape, structure and composition of the synthesized nanoparticles we have used FETEM and the elemental composition of the nanoparticle was determined using EDS mapping analysis. For this we diluted stock nanoparticles by 20X using HPLC grade water to a final concentration of  $\sim 0.5$  ppm (wrt  $\text{Cu}^{2+}$ ) and drop casted on TEM grid. It is worth mentioning that no TEM stain was used during preparation of the sample in order to visualize the presence of copper peroxide in the  $\text{CuPer}_{25}$ -BSA-NPs nanoparticles. The sample was dried under vacuum and subjected to TEM & EDS analysis.

**7. XPS analysis:** To confirm the oxidation states of the elements present (particularly oxygen) in the synthesized nanoparticles, X-ray photoelectron spectroscopy (XPS) experiment was performed. For this we have drop casted the nanoparticle solution on silicon wafer and dried under vacuum and subjected it to XPS analysis.

**8. Quantification of Cu in NPs:** To quantify the amount of Cu present in the synthesized nanoparticles we have used spectrophotometric method wherein we have used Patton's and Reeder's indicator to estimate the amount of copper present in the nanoparticles. Stock solution of  $\text{CuCl}_2 \cdot 2\text{H}_2\text{O}$  (100 ppm) was prepared by dissolving 10 mg of copper (II) salt in 0.5 N NaOH solution. The solution was neutralized using dil. HCl and the final volume was made up to 100 mL using 0.5 N NaOH solution. Patton's and Reeder's (HHSNNA) indicator (0.1 M) was prepared by dissolving the required amount of HHSNNA indicator in 0.5 N NaOH solution. Standard solutions containing variable Cu(II) concentrations (0 to 3 ppm) and 0.2 mM HHSNNA indicator were prepared in 0.25 N NaOH solution. Suitably diluted NP solutions were digested in conc.  $\text{HNO}_3$  and evaporated to dryness. The process was repeated for 3 times and the digested NPs were resuspended in 10 mL of 0.25 N NaOH solution containing 0.2 mM HHSNNA indicator. All the solutions were incubated in dark for 4 h. Absorbance of the standard and sample solutions were recorded at 545 nm. Concentration of Cu(II) in ppm was determined from an absorbance vs. concentration calibration curve for the standard solutions and were expressed in mean  $\pm$  SD.

**9. Release kinetics (pH dependent):** To determine the percentage of Cu released from the prepared  $\text{CuPer}_{25}$ -BSA-NPs in different pH (7.0 and 5.5) we have dialysed the NP solutions against acetate buffer of pH 7 and 5.5 and used aliquots from the dialysis bags at various time points to quantify Cu by spectrophotometric method. For this, we have diluted 1 mL of stock nanoparticles solution by 10X in distilled water and placed it in dialysis bags made out of

5000 Da cut-off membranes. The solutions were then dialyzed separately against acetate buffer of pH 7 and 5.5. Aliquots (500  $\mu\text{L}$ ) of the NP solution were withdrawn from the dialysis bags at suitable time points and evaporated to dryness. These were then digested 3 times using conc.  $\text{HNO}_3$  and re-suspended in 2 mL of 0.12 N NaOH solution containing 0.5 mM HHSNNA indicator. Absorbance of the samples were measured at 545 nm and converted to percentage of Cu(II) released from the NP solution by considering 0% release corresponding to the absorbance for NP solution withdrawn at 0 min. Results were expressed in % Cu(II) released  $\pm$  SD at various time points.

**10.pH dependent ROS generation studies by TMB assay:** To assess the pH dependent Reactive Oxygen Species (ROS) generation ability of the CuPer<sub>25</sub>-BSA-NPs, we have performed 3,3,5,5-tetramethylbenzidine (TMB) oxidation assay. TMB is known to oxidize under the influence hydroxyl radical to produce a bluish-green coloured compound, the production of which can be monitored by recording absorbance spectral peak at  $\sim$ 650 nm. A solution containing TMB (40  $\mu\text{g}/\text{mL}$ ) and the various concentrations (0, 0.2, 0.4, 1, 2 and 4 ppm w. r. t.  $\text{Cu}^{2+}$ ) of CuPer<sub>25</sub>-BSA-NPs in acetate buffer at pH 7.4 and 5.5 were incubated for 3 h at room temperature and absorbance of the solution was monitored at 650 nm. Control experiments were also performed to verify the role of Cu(II) and  $\text{H}_2\text{O}_2$  in TMB oxidation. For this, the above experiment was performed separately in presence of 1 mM of Cu(II), 1 mM of  $\text{H}_2\text{O}_2$  and a mixture of 1 mM Cu(II) and 1 mM  $\text{H}_2\text{O}_2$ .

We have performed TMB oxidation assays in buffer medium containing 1% and 10% fetal bovine serum (FBS) in order to evaluate the ROS generating capabilities of CuPer<sub>25</sub>-BSA-NPs in cell-mimicking environments. Each mL of FBS typically contains 3 – 7  $\mu\text{g}$  of glutathione<sup>1</sup>. It is evident from the experiments that the NPs are capable of generating ROS even in presence of FBS. At lower FBS concentrations (1%), the peak at  $\sim$ 650 nm (signifying the production of oxidized TMB) appears in the UV-vis spectra even for smaller concentrations of the NP but at higher concentrations of FBS (10%), due to the presence of very high intensity peaks at lower wavelengths, the peak at  $\sim$ 650 nm is masked. So, in order to see the peak at  $\sim$ 650 nm, higher NP concentrations were required. Nonetheless, appearance of bluish-green color with increase in NP concentrations was prevalent in all the various FBS-containing conditions confirming the ROS generating capabilities of CuPer<sub>25</sub>-BSA-NPs in cell-mimicking environments. The UV-vis spectra and representative images have been incorporated in the Figures S14 - S16.

**11. Kinetic studies of ROS production:** To determine the velocity of the generated hydroxyl radicals ( $\cdot\text{OH}$ ) from the CuPer<sub>25</sub>-BSA-NPs we have performed TMB oxidation assay with TMB concentrations ranging from 50  $\mu\text{M}$  to 350  $\mu\text{M}$  using 0.0323 ppm (wrt  $\text{Cu}^{2+}$ ) of CuPer<sub>25</sub>-BSA-NPs at pH 5.5 resulting in typical Michaelis-Menten kinetics curves. The Michaelis-Menten equation –

$$\frac{1}{V_0} = \frac{K_m}{V_{\max}[S]} + \frac{1}{V_{\max}}$$

Where  $V_0$  is the initial speed,  $V_{\max}$  is the maximum reaction speed.  $[S]$  is the substrate concentration (TMB) and  $K_m$  is the Michaelis-Menten constant.

According to derived Beer Lambert law, value of  $V_0$  was calculated by –

$$V_0 = \frac{A}{\epsilon_{650} \cdot b \cdot t}$$

Where  $A$  is the absorbance value at fixed time and 650 nm,  $\epsilon_{650}$  ( $39000 \text{ M}^{-1}\text{cm}^{-1}$ ) is the molar absorption coefficient of oxTMB, and  $b=1 \text{ cm}$ . The resulting data was fitted onto a Lineweaver-Burk ( $1/V$  vs.  $1/[\text{TMB}]$ ) plot. The  $V_{\max}$  was determined from the value of y-intercept.

**12. Quantification of generated ROS species:** To quantify the amount of  $\text{H}_2\text{O}_2$  generated from nanoparticles in acidic environment (pH 5.5) TMB oxidation assay was performed against various concentrations of TMB ranging from 100  $\mu\text{M}$  to 700  $\mu\text{M}$  (i.e. 20 ppm to 180 ppm) and keeping the nanoparticle concentration constant (4 ppm). From the absorbance (at 650 nm) vs. TMB concentration plot, the concentration of TMB at saturation condition was found to be 112 ppm. The amount of  $\text{H}_2\text{O}_2$  generated was calculated by considering stoichiometry of the components for a Fenton-like reaction involving copper.

**13. pH dependent  $\text{KMnO}_4$  decolorization Assay:** The intense purple colour of  $\text{MnO}_4^-$  is gradually diminishes as a result of its reduction to  $\text{Mn}^{2+}$  in presence of  $\text{H}_2\text{O}_2$  in an acidic environment. To further confirm the pH dependent  $\text{H}_2\text{O}_2$  generation capabilities of CuPer<sub>25</sub>-BSA-NPs,  $\text{KMnO}_4$  decolorization assay was performed at different pH. For this, we have prepared  $\text{KMnO}_4$  ( $50 \mu\text{g mL}^{-1}$ ) solution in two different pH conditions viz., 0.1 M  $\text{H}_2\text{SO}_4$  and acetate buffer (pH 7.4). The mixture was treated with varying concentrations (0, 0.2, 0.4, 1, 2 and 4 ppm w. r. t.  $\text{Cu}^{2+}$ ) of CuPer<sub>25</sub>-BSA-NP and incubated for 30 mins at room temperature. The UV-Vis spectra were recorded to monitor intensity of the peak at 550 nm.

**14. pH dependent stability analysis of the NPs by DLS studies:** To determine the stability of CuPer<sub>25</sub>-BSA-NPs at different pH, Dynamic light scattering (DLS) measurements were performed. For this we have diluted the CuPer<sub>25</sub>-BSA-NPs solution by 5X in acetate buffer adjusted to various pH (8.0, 7.0, 7.4, 6.0, 5.5 and 5.0) and the resultant solution was subjected to DLS measurements. Size and zeta potentials were monitored and represented as a function of pH so as to detect any drastic changes resulting from nanoparticle agglomeration and disassociation.

**15. Cellular cytotoxicity studies:** Cytotoxicity of the CuPer<sub>25</sub>-BSA-NPs was studied in RAW 264.7 cells using MTT assay. RAW 264.7 macrophages (5000 cells/well) were seeded on a 96-well plate and allowed to grow 24 h at 37 °C in 5% CO<sub>2</sub>. CuPer<sub>25</sub>-BSA-NPs were added to the cells in fresh DMEM and incubated for 4 h. Media was aspirated from the wells and fresh media was added and the cells were incubated for another 24 h following which, MTT (5 mg/mL, 20 µL/well) was added to the wells. The plates were then incubated for another 4 h for the conversion of MTT to formazan by cellular reductase enzymes. The media was removed and cells were lysed using 100 µL of DMSO and homogenized with gentle shaking at room temperature. The absorbance of the resultant solution in each well was read at 550 nm with a background reading at 800 nm. Cytotoxicity was expressed as mean percentage increase relative to the untreated control ± standard deviation. Control values were set at 0% cytotoxicity or 100% cell viability. Cytotoxicity data was fitted to a sigmoidal curve and a three parameters logistic model used to calculate the inhibitory concentration-50 (IC<sub>50</sub>) that is the concentration of test article under investigation showing 50% inhibition in comparison to untreated controls. These analyses were performed with GraphPad Prism (San Diego, U.S.A).

**16. DCFDA assay:** Intracellular ROS levels in CuPer<sub>25</sub>-BSA-NPs treated RAW 264.7 cells were assessed using the 2',7' -dichlorofluoresceindiacetate (DCFDA) assay which after the action of cellular esterases and oxidation by ROS turns into fluorescent 2', 7' -dichlorofluorescein (DCF). This dye internalizes into the cells, gets deacetylated under the influence of cellular esterases and finally oxidized itself to 2',7'-Dichlorofluorescein (DCF) in presence of reactive oxygen species. The fluorescence of DCF can be monitored spectroscopically at  $\lambda_{ex}/\lambda_{em}$  at 485/535 nm and it gives a measure of the ROS levels. RAW 264.7 cells were plated in 6 well plates at a cell density of 5 X 10<sup>5</sup> cells/well and were treated with 100 µM of DCFH<sub>2</sub>-DA in DMEM and incubated for 30 min at 37 °C in 5% CO<sub>2</sub>. Supernatant media was aspirated and the cells were washed with 1X PBS for three times. Cell was then incubated with 1 ppm (w. r. t. Cu<sup>2+</sup>) CuPer<sub>25</sub>-BSA-NPs for 2h 37 °C in 5% CO<sub>2</sub>.

Cells were washed again with 1X PBS for three times and lysed with 1 mL of 90% (v/v) DMSO solution in 1X PBS for 10 min in dark at room temperature. Fluorescence intensity of the cell lysates was measured using a fluorescence spectrophotometer at  $\lambda_{\text{ex}}/\lambda_{\text{em}}$  at 485/535 nm.

**17. Quantification of intracellular nitrite concentration in macrophages:** To perform the assay,  $5 \times 10^5$  cells/well of RAW 264.7 cells were plated in 6 well plates and allowed to adhere to the plate for overnight. Cells were then either kept untreated or treated with BSA-NPs or 1 ppm (w. r. t.  $\text{Cu}^{2+}$ ) CuPer<sub>25</sub>-BSA-NPs for 4h 37 °C in 5% CO<sub>2</sub>. Cells were then washed with 1X PBS for three times and allowed to incubate in fresh media for 24 h. Media was removed, cells were washed with 1X PBS and lysed using a 1 mL (per well) lysis buffer containing 10 mM boric acid and 2 mM TTAC at pH 10.3 to 10.7. Lysates were then centrifuged at 5000 rpm for 5 min to get rid of any debris and 500  $\mu\text{L}$  of each of the lysates was added into 500  $\mu\text{L}$  of Griess reagent, left to react for 15 min, after which the absorbance at 540 nm was recorded using UV-vis spectrophotometer. A buffer background was always employed for these measurements. For nitrite quantitation, a calibration curve was prepared using nitrite standards from 1 to 50  $\mu\text{M}$ . Cell counts were taken before lysing the cells, and the final nitrite concentration was normalized with respect to the cell counts.

**18. Immunostaining of macrophages:** Macrophages express biomarkers specific to its phenotype and meticulous monitoring of these biomarkers utilizing suitable techniques enable identification of associated phenotypes. Immunostaining CuPer<sub>25</sub>-BSA-NPs treated macrophages with suitable biomarkers and visualizing them under microscope would enable us to understand the type of polarization brought about by the NPs. To perform immunostaining experiments, RAW 264.7 cells were plated at a cell density of 20,000 cells per well on glass coverslips placed in a 12-well plate and were allowed to adhere on the coverslips for overnight. Media was removed from the wells and the cells were then treated with CuPer<sub>25</sub>-BSA-NPs (1 ppm w.r.t.  $\text{Cu}^{2+}$ ) and allowed to incubate at 37 °C for 2 h. After 2 h in absence or presence of NPs, the media was aspirated out, washed and fixed with 4% paraformaldehyde for 15 min at room temperature, and permeabilized using 0.2% Triton-X for 10 min. Cells were washed with 1X PBS for 3 times and blocked with 10% goat serum in 1X PBS for 6 h. Cells were washed thrice with 1X PBS and treated with Allophycocyanin (APC)-conjugated monoclonal rat primary antibody against murine CD206 and Alexa Fluor 488-conjugated monoclonal rat antibody against murine iNOS at a dilution of 1/1000 in 10% goat serum containing 1X PBS for 12 h at 4 °C. After washing the cells for three more times

with 1X PBS, they were mounted on glass slides with mounting solution and imaged under Zeiss ApoTome inverted fluorescence microscope.

**19. Toxicity of conditioned media in HeLa cells:** RAW 264.7 cells were plated in 35 mm culture dishes at a cell density of 500,000 cells per dish and were allowed to incubate overnight. Media was removed from the wells and the cells were then treated with fresh media, BSA-NPs and CuPer<sub>25</sub>-BSA-NPs (1 ppm w.r.t. Cu<sup>2+</sup>) and allowed to incubate at 37 °C for 4 h. After 4 h the media was aspirated out, washed with 1X PBS for 3 times and incubated with fresh media for another 24 h. At this point, HeLa cells were plated in a 96 well plate at a cell density of 3000 cells per well and allowed to grow for 24 h at 37 °C. Conditioned supernatant media was collected from the three petri dishes and centrifuged at 3000 rpm for 5 minutes to get rid of any suspended cells and debris. Supernatant media from the HeLa cells in the 96 well plate was removed and the cells were treated with fresh media or a 1:3 composition (in fresh media) of conditioned media from untreated RAW 264.7 cells, RAW 264.7 cells treated with BSA-NPs, RAW 264.7 cells treated with CuPer<sub>25</sub>-BSA-NPs. The HeLa cells were then incubated for another 24 h post which, viability of the cells was assessed by MTT assay. Results were represented in percentage ( $\pm$  standard deviation) considering 100% cell viability for untreated HeLa cells.

**20. Statistical Analyses:** All statistical analyses were performed using GraphPad Prism software performing a one-way analysis of variance (ANOVA) and nonparametric analyses followed by the Tukey post test. The p-values (wherever applicable) have been mentioned in the respective figure captions.

**21. Comparison of reported literature on ROS generating NPs for macrophage polarization with the research work presented herein:** In order to highlight the novelty aspect of the research work presented herein we have tabulated below (Table S1) the various nanoparticles reported in literature that have been used for polarization of macrophages via generation of ROS with CuPer-BSA-NPs. Various metallic NPs, oxide NPs, polymeric NPs and MOFs have been used to modulate macrophages via generation of different ROS. It is evident that while a variety of nanoparticles have been used for such applications among which there are some Cu-based particles too but, to the best of our knowledge, this is the first report wherein copper peroxide has been stabilized in BSA nanoparticles and its self-supplying, pH-dependent ROS generating abilities have been used for macrophage modulation and immunotherapeutic application.

**Table S1** Comparison of reported ROS-generating NPs used for polarization of macrophages with CuPer-BSA-NPs (present work)

SL No	Nanoparticles	Core	Coating	Type of ROS generated	Mechanism	Model/Cell lines	References
1.	Amorphous silica nanoparticles	SiO <sub>2</sub>	---	NS*	pro-inflammatory responses in vivo/in vitro	RAW 264.7 cells and ICR mice	<i>Toxicol. Lett.</i> , 2009, <b>184</b> , 18–25 <sup>2</sup>
2.	Mouse serum albumin (MSA) coated AuNPs (AuNP-MSA) and AgNPs (AgNP-MSA)	AuNPs/AgNPs	Mouse Serum Albumin (MSA)	Superoxide radical	polarization from M2 to M1 phenotype of TAMs in vivo	LACA male Swiss albino mice	<i>Int. Immunopharmacol.</i> , 2016, <b>38</b> , 332–341 <sup>3</sup>
3.	Amino-functionalized polystyrene nanoparticles	---	Amino-functionalized polystyrene	NS*	Induction of NLRP3 inflammasome activation and subsequent IL-1 $\beta$ production by human macrophages	Human monocyte differentiated to macrophages using M-CSF	<i>ACS Nano</i> , 2011, <b>5</b> (12), 9648–9657 <sup>4</sup>
4.	ultrafine (uf) TiO <sub>2</sub> or fine crystalline silica (DQ12 quartz)	TiO <sub>2</sub> /SiO <sub>2</sub>	---	NS*	pro-inflammatory responses in vitro	NR8383 rat Alveolar Macrophages	<i>Particle and Fibre Toxicol.</i> , 2011, <b>8</b> :31 <sup>5</sup>
5.	Titanium Dioxide Nanoparticles	TiO <sub>2</sub>	---	NS*	activation of TH <sub>1</sub> and TH <sub>2</sub> response	Spleenocyte macrophages from Wistar rats	<i>Appl. Biochem. biotechnol.</i> , 2016, <b>180</b> , 1257-1275 <sup>6</sup>
6.	CeO <sub>2</sub> nanoparticles	CeO <sub>2</sub>	---	NS*	Release of pro-inflammatory and fibrotic cytokines in vivo	Branchoalveolar macrophages of Sprague-Dawley (Hla:SD-CVF) rats	<i>Nanotoxicol.</i> , 2011, <b>5</b> , 312-25 <sup>7</sup>
7.	ZnO nanoparticles	ZnO	---	NS*	Polarization of macrophages to M1 phenotype	RAW 264.7 cells	<i>ACS Appl. Mater. Interfac.</i> , 2017, <b>9</b> , 39971-39984 <sup>8</sup>
8.	SPION	Fe <sub>3</sub> O <sub>4</sub>	---	NS*	Promotes M1 polarization in M2 macrophages	THP-1 cells	<i>Nanomed.: Nanotechnol. Biol. Med.</i> , 2016, <b>12</b> , 1127-1138 <sup>9</sup>
9.	PEI-coated SPIONs (PMag)	Fe <sub>3</sub> O <sub>4</sub>	Polyethyleneimine	NS*	Induction of M1 phenotype in TLR4 and ROS dependent manner	Peritoneal macrophages from female C57BL/6J mice	<i>Biomater.</i> 2015, <b>52</b> , 494-506 <sup>10</sup>
10.	Ferumoxytol	Fe <sub>3</sub> O <sub>4</sub>	---	H <sub>2</sub> O <sub>2</sub> and $\cdot$ OH	Polarization of murine macrophages (in-vitro) and TAMs (in-vivo) towards M1 phenotype	RAW 264.7 cells and female FVB/N mice	<i>Nat. Nanotechnol.</i> , 2016, <b>11</b> , 986-994 <sup>11</sup>

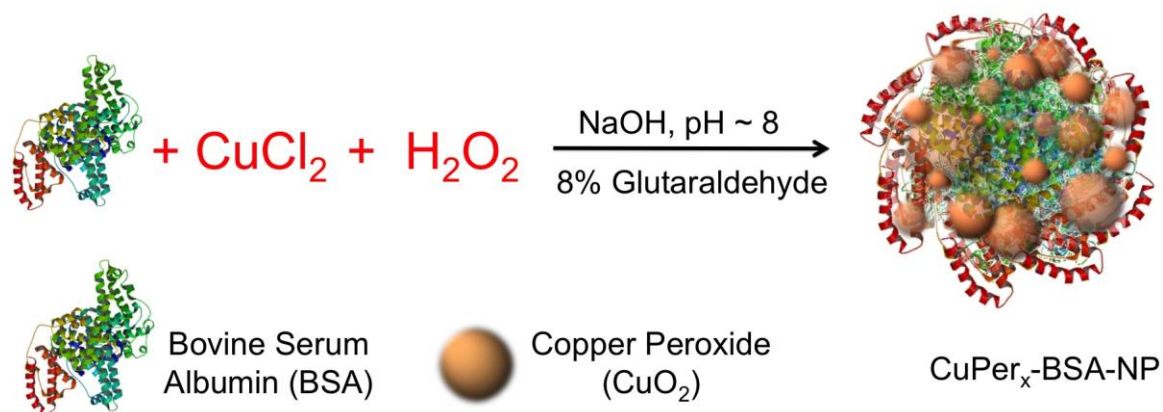
11.	Carboxy-dextran coated SPION	Fe <sub>2</sub> O <sub>3</sub> and Fe <sub>3</sub> O <sub>4</sub>	Carboxy-dextran	NS*	phenotypic shift in M2 macrophages towards M1	THP1 derived M2 macrophages	<i>Biochem. Biophys. Res. Commun.</i> , 2013, <b>441</b> , 737-742 <sup>12</sup>
12.	Gold nanocages loaded DOX and BSO with surface camouflage of 4 T1 cell membranes (m@Au-D/B NCs)	Gold nanocage loaded doxorubicin (DOX) and l-buthionine sulfoximine (BSO)	4T1 cell membranes	•OH, and O <sub>2</sub> •-	Repolarization of tumor-associated macrophages (TAMs) from pro-tumor (M2) phenotype to anti-tumor (M1) phenotype	BALB/c mice	<i>J. Colloid Interface Sci.</i> , 2022, <b>606</b> , 1950-1965 <sup>13</sup>
13.	PEGylated Iron Manganese silicate NPs loaded with TGFβ inhibitor (SB-505124)	Iron Manganese silicate	PEG	•OH, <sup>1</sup> O <sub>2</sub>	Macrophage polarization from M2 to M1 in-vivo	CT26-tumor-bearing mice	<i>Adv. Mater.</i> 2020, <b>32</b> (33), 2003563 <sup>14</sup>
14.	Rhodamin110-BSA @ PSiNPs	Porous Si nanoparticles	BSA	Mitochondrial ROS and superoxide	M1 polarization	RAW 264.7 macrophages	<i>ACS Nano</i> , 2023, <b>17</b> , 1036–1053 <sup>15</sup>
15.	Ultra-small Se@ZIF-8 core-satellite nanoassembly	Se nanoparticles and Zn <sup>2+</sup>		•OH	Reprogramming Tumor-Associated Macrophages	RAW 264.7 macrophages and Tumor bearing Balb/C mice	<i>Nano Lett.</i> ,2024, <b>24</b> (29), 9104-9114 <sup>16</sup>
16.	PMA@Fe <sub>3</sub> O <sub>4</sub>	Fe <sub>3</sub> O <sub>4</sub>	PMA	NS*	M0 to M1	RAW 264.7 macrophages	<i>Nanoscale</i> 2019, <b>11</b> (47), 22849-22859 <sup>17</sup>
17.	Ferumoxytol	Fe <sub>2</sub> O <sub>3</sub>	PSC	•OH	M0 to M1	RAW 264.7 macrophages, BALB/c mice	<i>Biomater.</i> , 2019, <b>203</b> , 23-30 <sup>18</sup>
18.	PEG-coated ferrihydrite nanoparticles (PEG-Fns)	Ferrihydrite nanoparticles	PEG	NS*	M0 to M1	RAW 264.7 macrophages	<i>Biomater.</i> , 2021, <b>271</b> , 120739 <sup>19</sup>
19.	CuONPs	CuO	---	•OH	NLRP3 inflammasome activation and IL-1β secretion in J774A.1 macrophages	J774A.1 macrophage	<i>J. Hazard. Mater.</i> ,2021, <b>411</b> , 125134 <sup>20</sup>
20.	CuTCPP@MOF nanodots@ Mannosamine (CTMM)	Cu-porphyrin MOF	D-Mannosamine	NS*	SDT driven Pro-inflammatory polarization	RAW 264.7 cells	<i>Nano Today</i> 2024, <b>54</b> , 102092 <sup>21</sup>
21.	CuS NP	CuS	---	•OH	M1 Polarization	Bone marrow derived macrophages	<i>Adv. Funct. Mater.</i> ,2021, <b>31</b> (11), 2008022 <sup>22</sup>
22.	CuS@OVA	CuS	Ovalbumin	NS*	PTT assisted M1 Polarization in TAMs	RAW 264.7 macrophages	<i>Acta Biomater.</i> , 2023, <b>167</b> , 551-563 <sup>23</sup>

23.	CuPer-BSA-NPs	Copper Peroxide	BSA	Self-supplying source of Cu <sup>2+</sup> and H <sub>2</sub> O <sub>2</sub> . Resultant ·OH generation via Fenton-like mechanism	M0 to M1 Polarization and anti-cancer effect of conditioned media from M1 polarized macrophages on HeLa cells	RAW 264.7 macrophages	<i>This research work</i>
-----	---------------	-----------------	-----	--	---	-----------------------	---------------------------

\*NS: Not Specified

**Table S2** Size and zeta potential of the Nanoparticles.

Name of the NPs	Mean size (nm) $\pm$ SD	Zeta Potential (mV) $\pm$ SD
BSA-NP	309.7 $\pm$ 14.0	-11.13 $\pm$ 1.48
CuPer <sub>12.5</sub> -BSA-NPs	53.4 $\pm$ 0.26	8.98 $\pm$ 1.01
CuPer <sub>25</sub> -BSA-NPs	59.2 $\pm$ 0.95	11.47 $\pm$ 1.94
CuPer <sub>50</sub> -BSA-NPs	33.7 $\pm$ 0.32	5.93 $\pm$ 1.67
CuPer <sub>75</sub> -BSA-NPs	42.9 $\pm$ 0.63	9.96 $\pm$ 2.65



**Scheme S1** Schematic representation of the synthetic approach for  $\text{CuPer}_x\text{-BSA-NPs}$ .

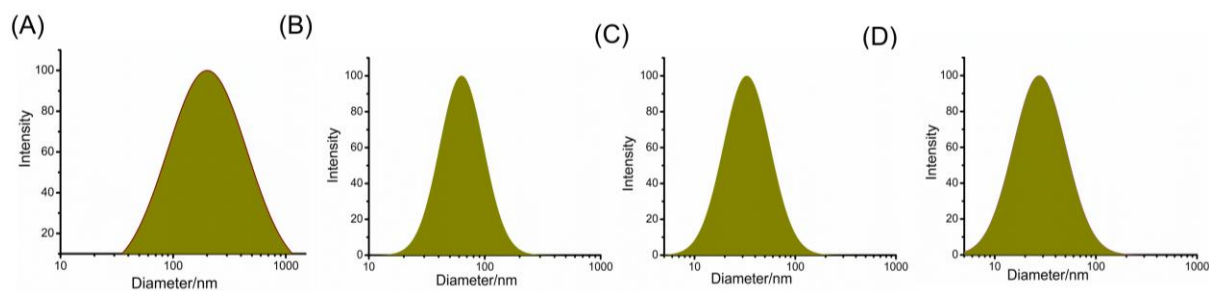


**Figure S1.** DLS size histogram obtained for (A) BSA-NP, (B) CuPer<sub>12.5</sub>-BSA-NP, (C) CuPer<sub>50</sub>-BSA-NPs and (D) CuPer<sub>75</sub>-BSA-NPs.

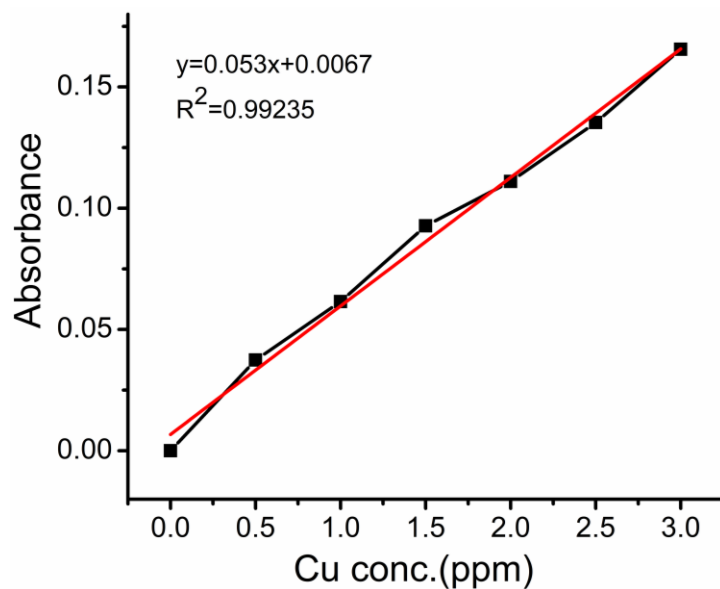


**Figure S2.** Representative Calibration curve for Cu Quantification showing equation and  $R^2$  values.

**Table S3** Percentage Loading (% L), percentage Incorporation Efficiency (% IE) and concentration (in ppm) of Cu present in the nanoparticles

Name	% Loading	% Incorporation Efficiency	Cu concentration (ppm)
BSA-NP	---	---	---
CuPer <sub>12.5</sub> -BSA-NP	1.78	3.78	5.56 ± 0.21
CuPer <sub>25</sub> -BSA-NP	2.84	6.10	9.68 ± 1.08
CuPer <sub>50</sub> -BSA-NP	3.91	8.54	13.55 ± 0.71
CuPer <sub>75</sub> -BSA-NP	5.65	12.52	19.85 ± 3.55

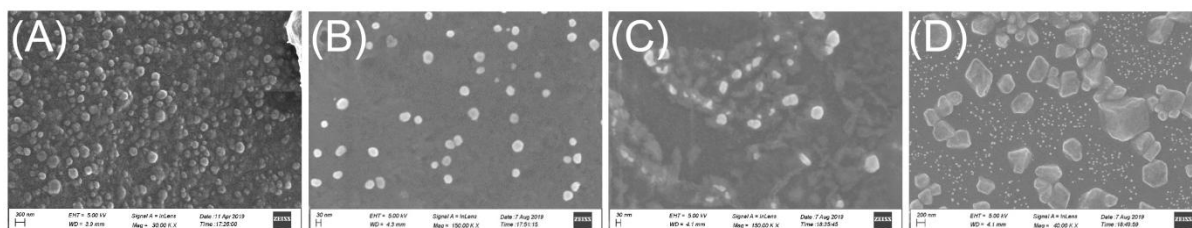


**Figure S3.** SEM images obtained for (A) BSA-NP (B) CuPer<sub>12.5</sub>-BSA-NP (C) CuPer<sub>50</sub>-BSA-NPs and (D) CuPer<sub>75</sub>-BSA-NPs. Scale bar for (A) correspond to 300 nm, for (B) and (C) correspond to 30 nm and that for (D) corresponds to 200 nm.

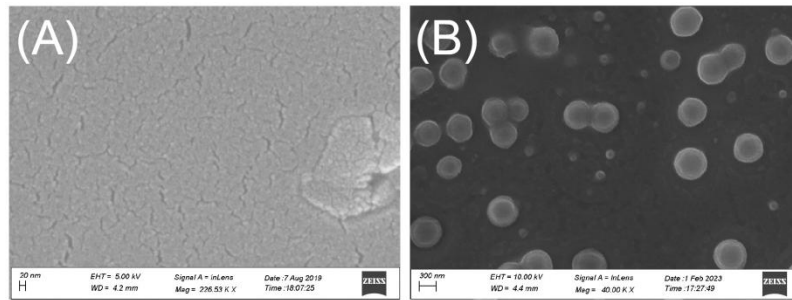


**Figure S4.** SEM images obtained for solutions from control nanoparticle synthesis experiments wherein all the other conditions were kept same as that for CuPer<sub>x</sub>-BSA-NP, but in (A) CuCl<sub>2</sub> was not added and in (B) BSA was not added. Scale bar for (A) corresponds to 30 nm while that for (B) corresponds to 300 nm.

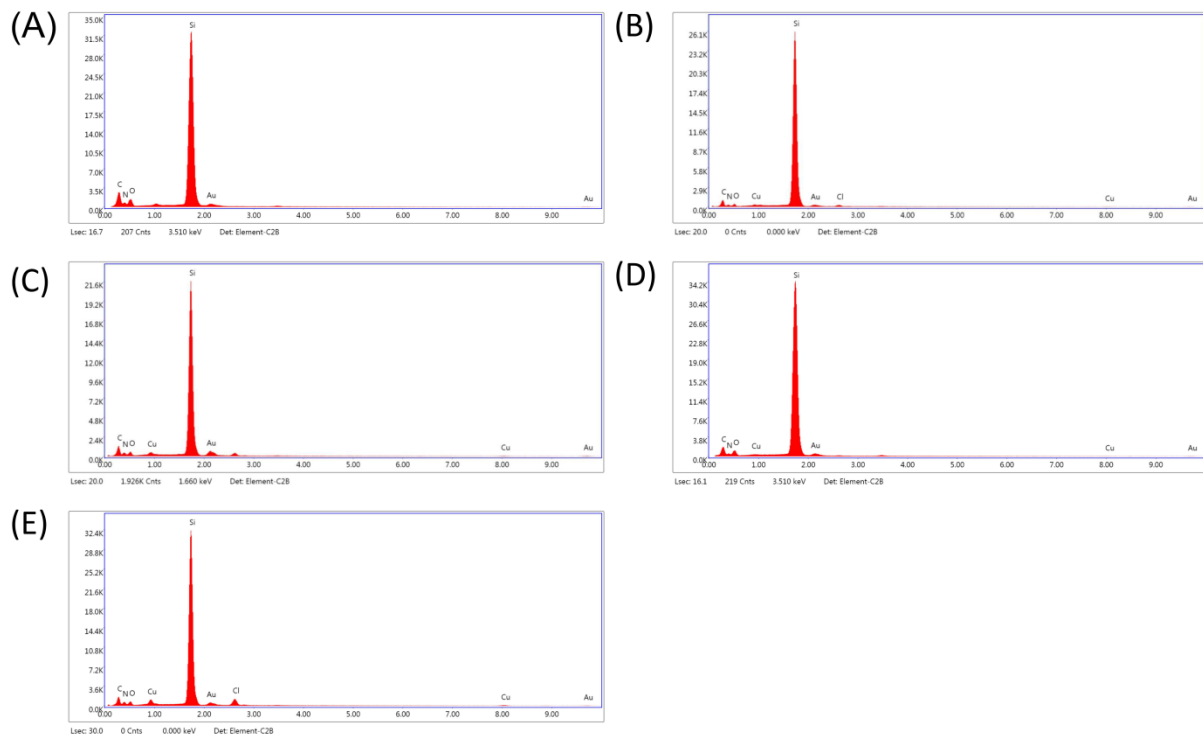


**Figure S5.** Energy dispersive X-ray analysis (EDAX) of silicon wafers coated with (A) BSA-NP (B) CuPer<sub>12.5</sub>-BSA-NP (C) CuPer<sub>25</sub>-BSA-NP (D) CuPer<sub>50</sub>-BSA-NPs and (E) CuPer<sub>75</sub>-BSA-NPs.

**Table S4** Surface composition of the nanoparticles as obtained from EDAX analyses

Element	BSA-NP		CuPer <sub>12.5</sub> -BSA-NP		CuPer <sub>25</sub> -BSA-NP		CuPer <sub>50</sub> -BSA-NP		CuPer <sub>75</sub> -BSA-NP	
	Weight %	Atom %	Weight %	Atom %	Weight %	Atom %	Weight %	Atom %	Weight %	Atom %
C K	53.44	62.00	20.37	37.35	23.58	41.36	34.23	48.21	21.06	37.73
N K	17.91	17.81	1.97	3.09	5.47	8.23	18.02	21.76	5.77	8.86
O K	20.58	17.92	1.65	2.26	3.35	4.41	17.36	18.35	3.11	4.18
Cu K	---	---	1.08	0.37	1.87	0.62	7.53	2.01	3.54	1.20

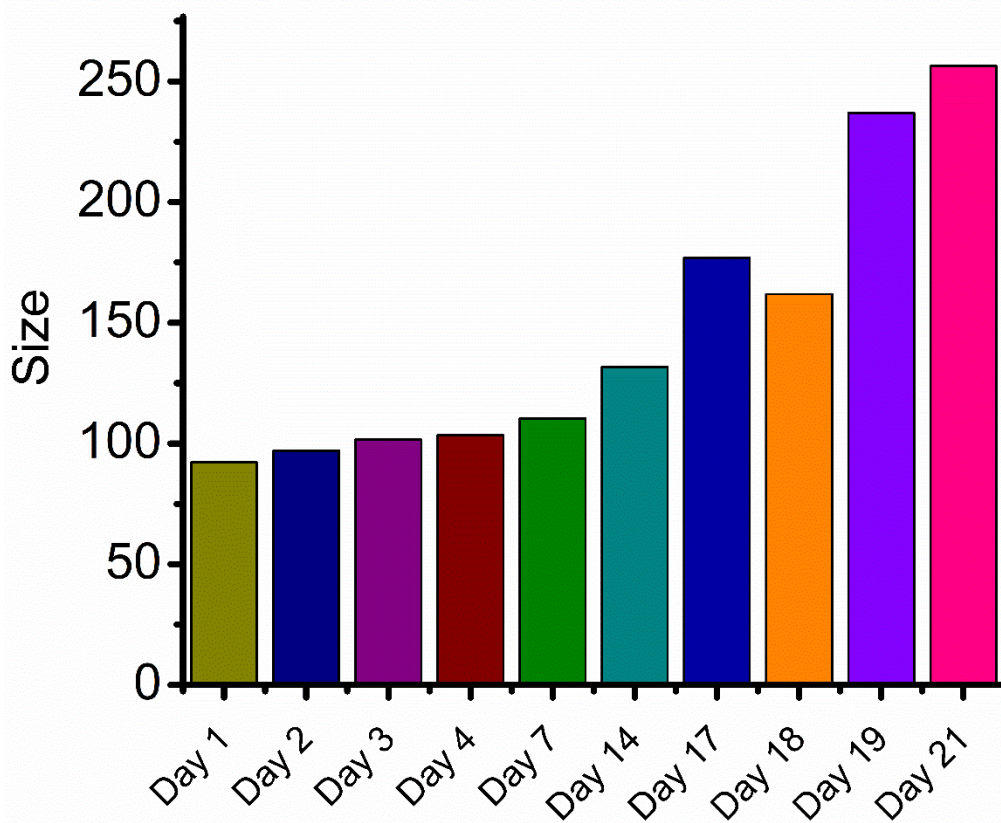


**Figure S6.** Time-dependent stability study for CuPer<sub>25</sub>-BSA-NPAs determined by size measurements over 3 weeks using DLS instrument.

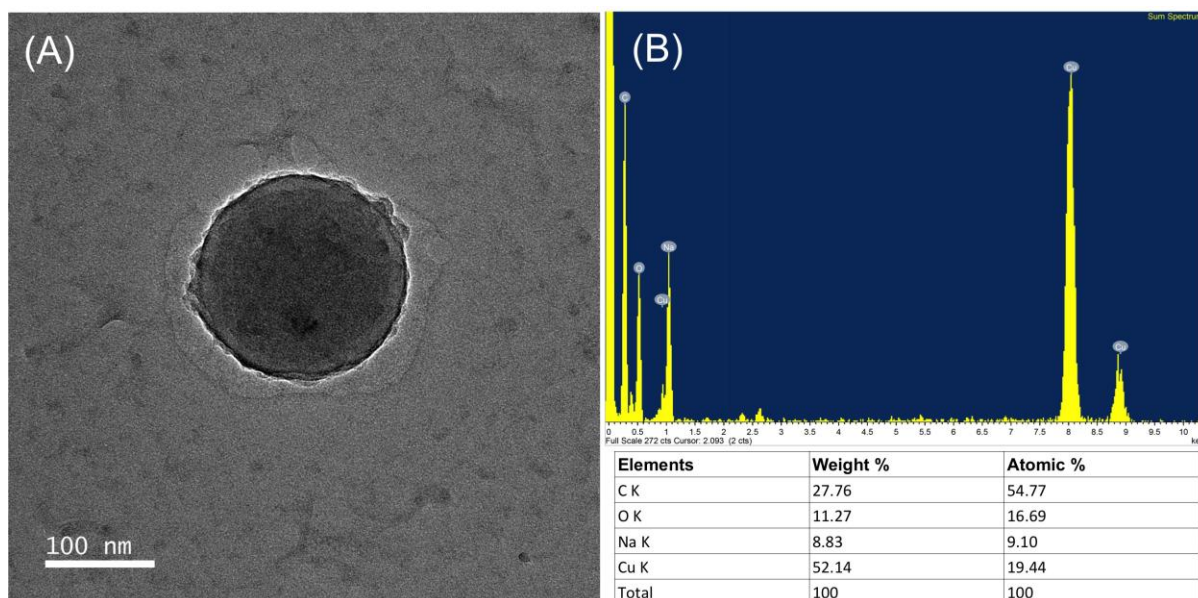


**Figure S7.** (A) TEM image and (B) EDS mapping data & content analysis of CuPer<sub>25</sub>-BSA-NPs.

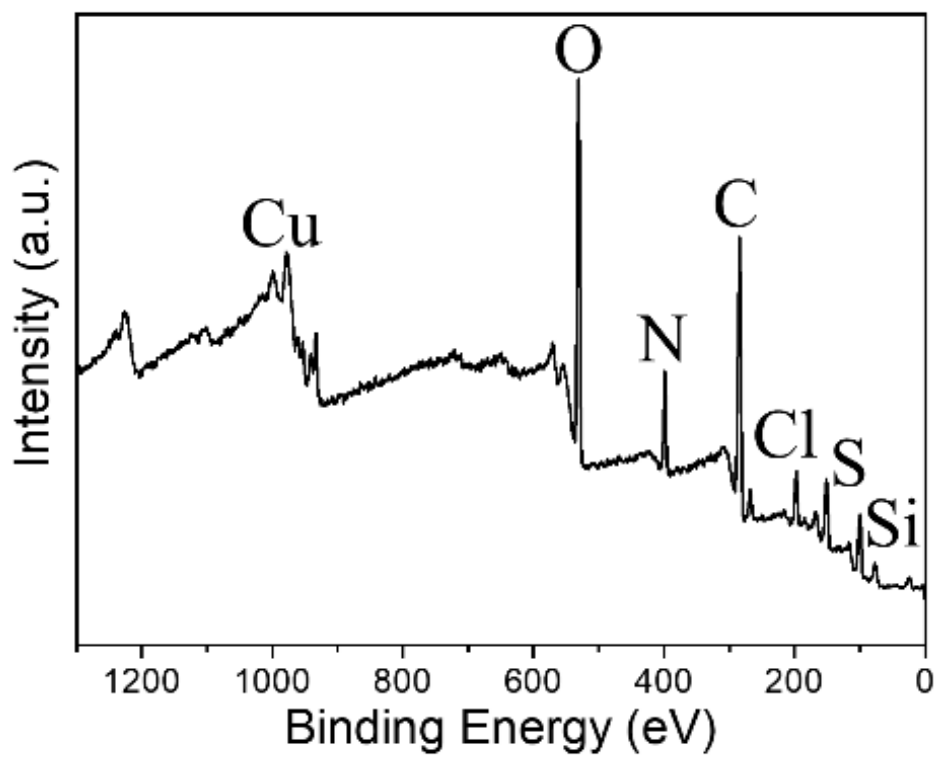


**Figure S8.** Full range X-ray Photoelectron Spectrum of CuPer<sub>25</sub>-BSA-NPs.

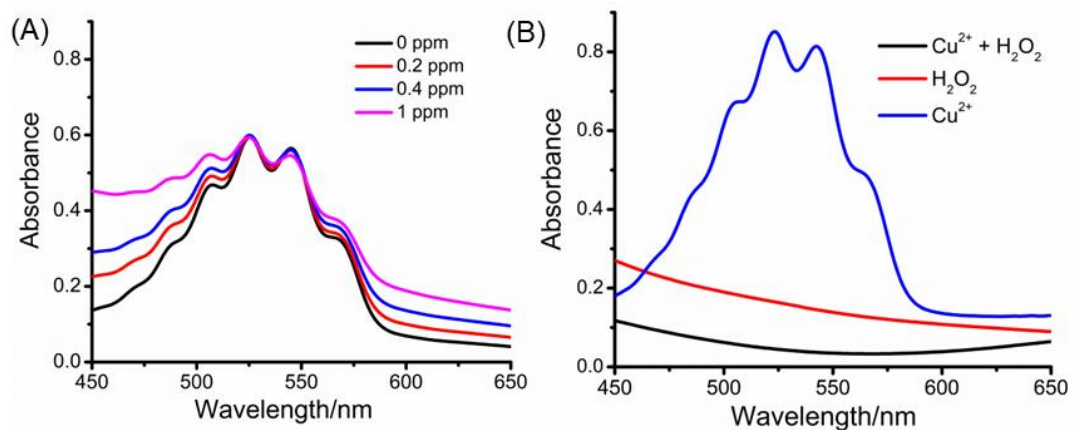


**Figure S9.** Control KMnO<sub>4</sub> decolorization experiments (A) in presence of CuPer<sub>25</sub>-BSA-NPs at pH 7.4 (B) in presence of free Cu<sup>2+</sup> (1 mM), H<sub>2</sub>O<sub>2</sub> (1 mM) and a mixture of Cu<sup>2+</sup> & H<sub>2</sub>O<sub>2</sub> (1 mM each) in acidic pH.

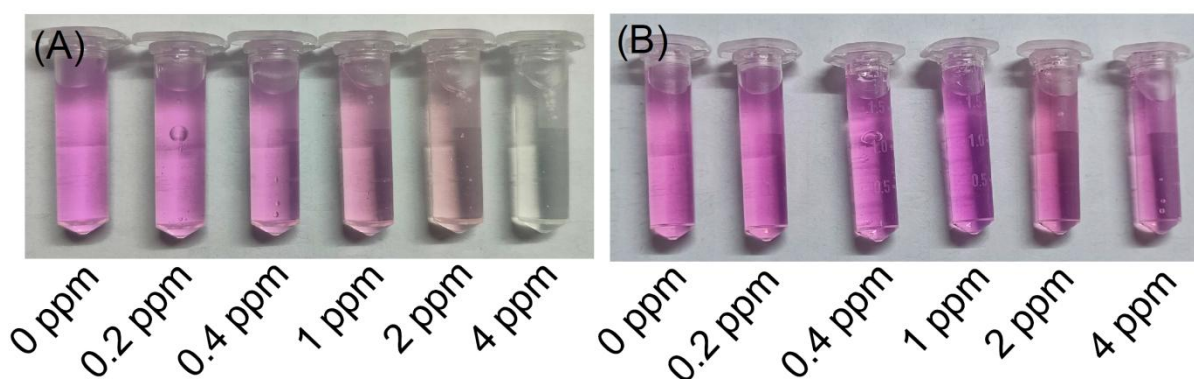


**Figure S10.** Representative images for the solutions in a KMnO<sub>4</sub> decolorization assay in presence of CuPer<sub>25</sub>-BSA-NPs (A) in acidic pH and (B) at pH 7.4.

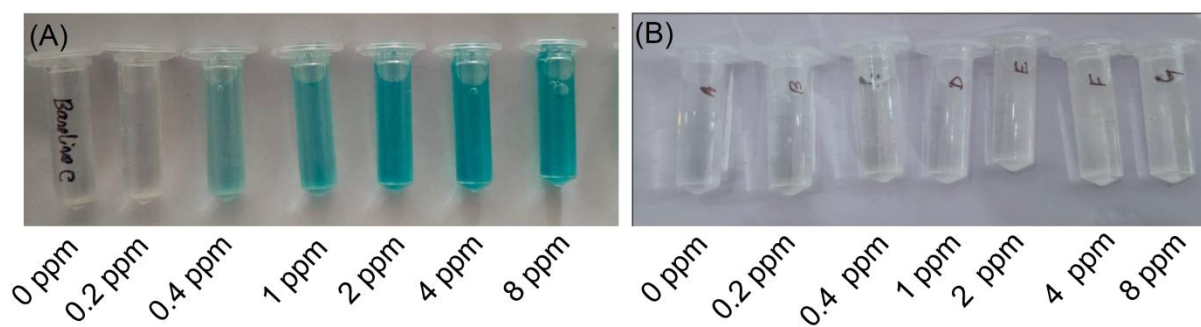


**Figure S11.** Representative images for the solutions in a TMB oxidation assay in presence of CuPer<sub>25</sub>-BSA-NPs (A) in acidic pH 5.5 and (B) at pH 7.4.

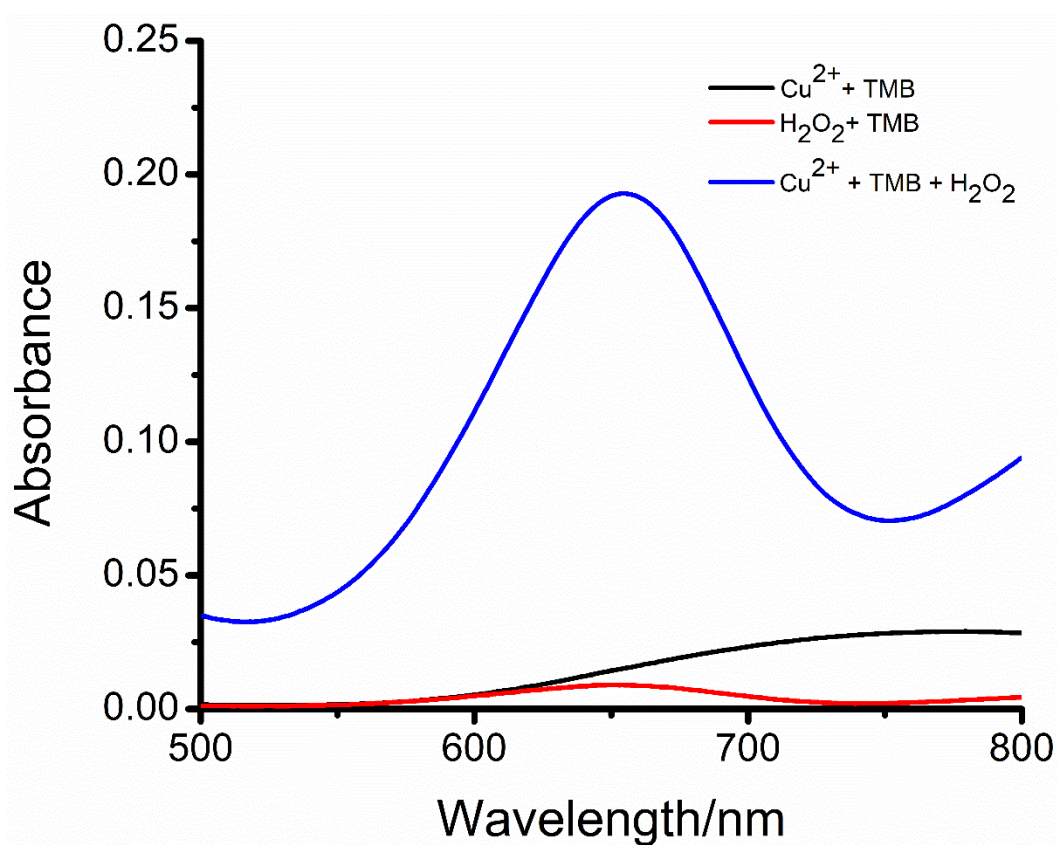


**Figure S12.** Control TMB oxidation experiments at pH 5.5 in presence of free Cu<sup>2+</sup> (1 mM), H<sub>2</sub>O<sub>2</sub> (1 mM) and a mixture of Cu<sup>2+</sup> & H<sub>2</sub>O<sub>2</sub> (1 mM each).

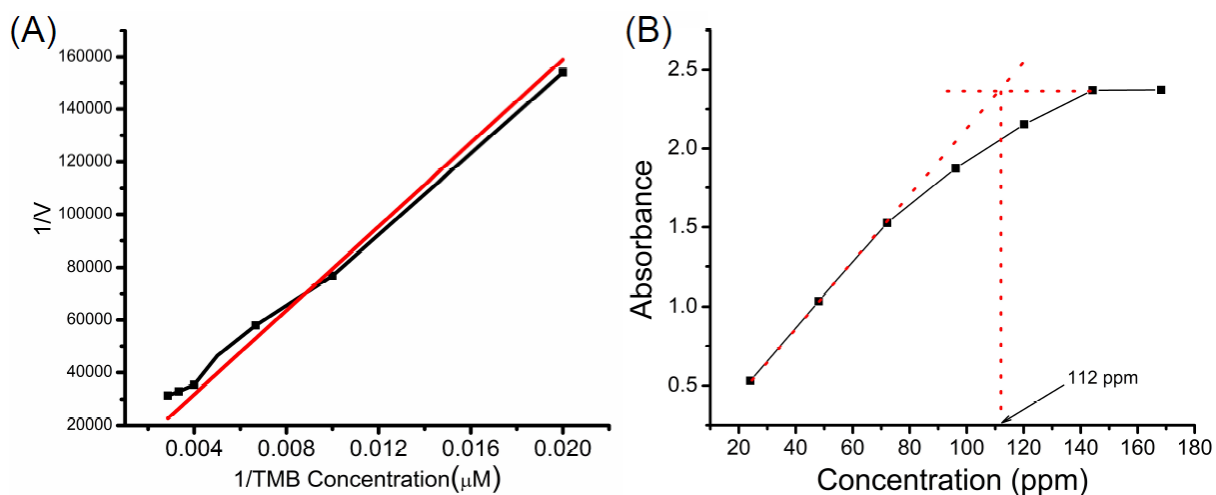


**Figure S13.** (A) Lineweaver-Burk plot for steady-state kinetic study of CuPer<sub>25</sub>-BSA-NP at variable TMB concentrations in Sodium acetate buffer solution (pH = 5.5). (B) TMB oxidation assay performed using 0.0323 ppm (wrt Cu<sup>2+</sup>) of CuPer<sub>25</sub>-BSA-NPs with increasing TMB concentrations (20-180 ppm) for determination of the amount of H<sub>2</sub>O<sub>2</sub> produced.

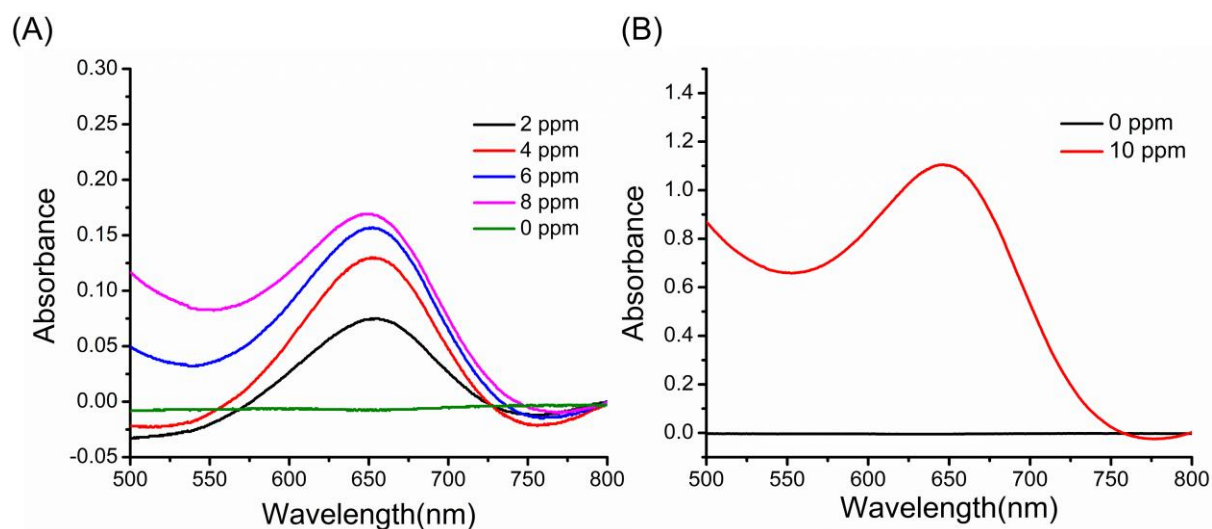


**Figure S14.** UV-vis spectra for TMB oxidation assays in presence of (A) 1% and (B) 10% Fetal Bovine Serum (FBS) at various CuPer<sub>25</sub>-BSA-NP concentrations.

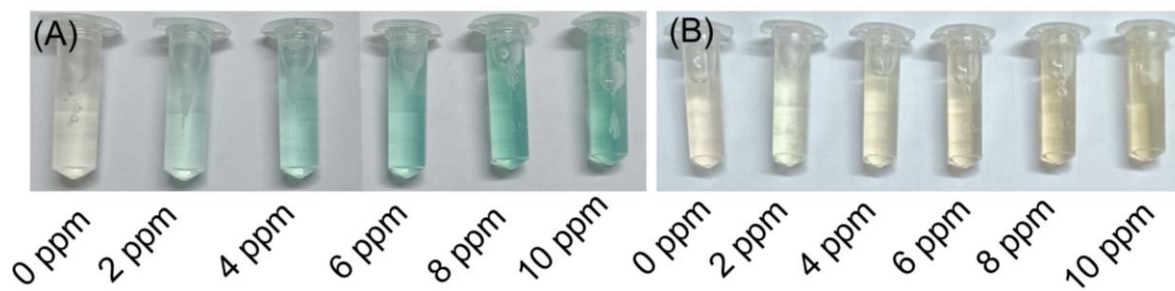


**Figure S15.** Representative images for the solutions in a TMB oxidation assay in presence of 1% Fetal bovine serum (FBS) using CuPer<sub>25</sub>-BSA-NPs at (A) pH 5.5 and (B) pH 7.4.

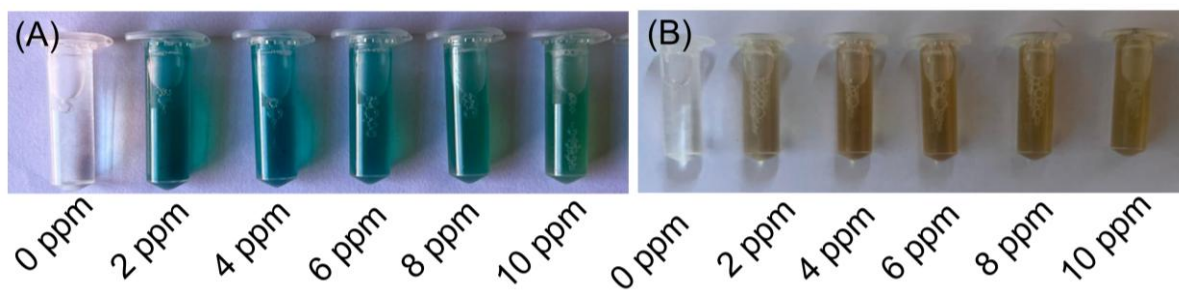


**Figure S16.** Representative images for the solutions in a TMB oxidation assay in presence of 10% Fetal bovine serum (FBS) using CuPer<sub>25</sub>-BSA-NPs (A) in acidic pH 5.5 and (B) at pH 7.4.

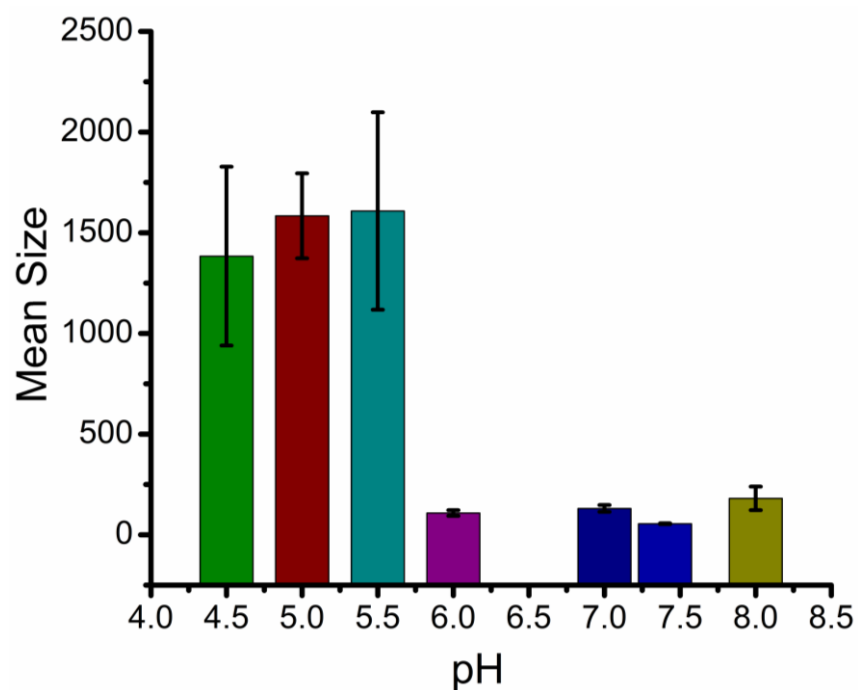


**Figure S17.** pH-dependent stability study for CuPer<sub>25</sub>-BSA-NP as determined by size measurements over a pH range of 4.5 – 8.0 using DLS instrument.

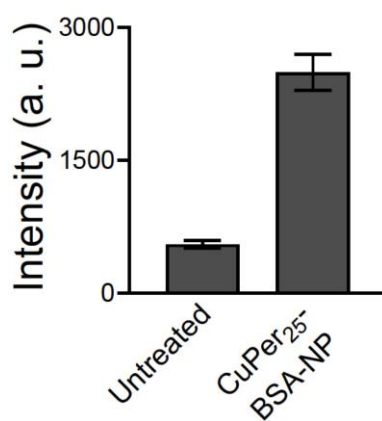


**Figure S18.** Fluorescence intensity of DCF depicting ROS levels in RAW 264.7 cells upon treatment with ~0.5 ppm CuPer<sub>25</sub>-BSA-NPs in comparison to the untreated ones.

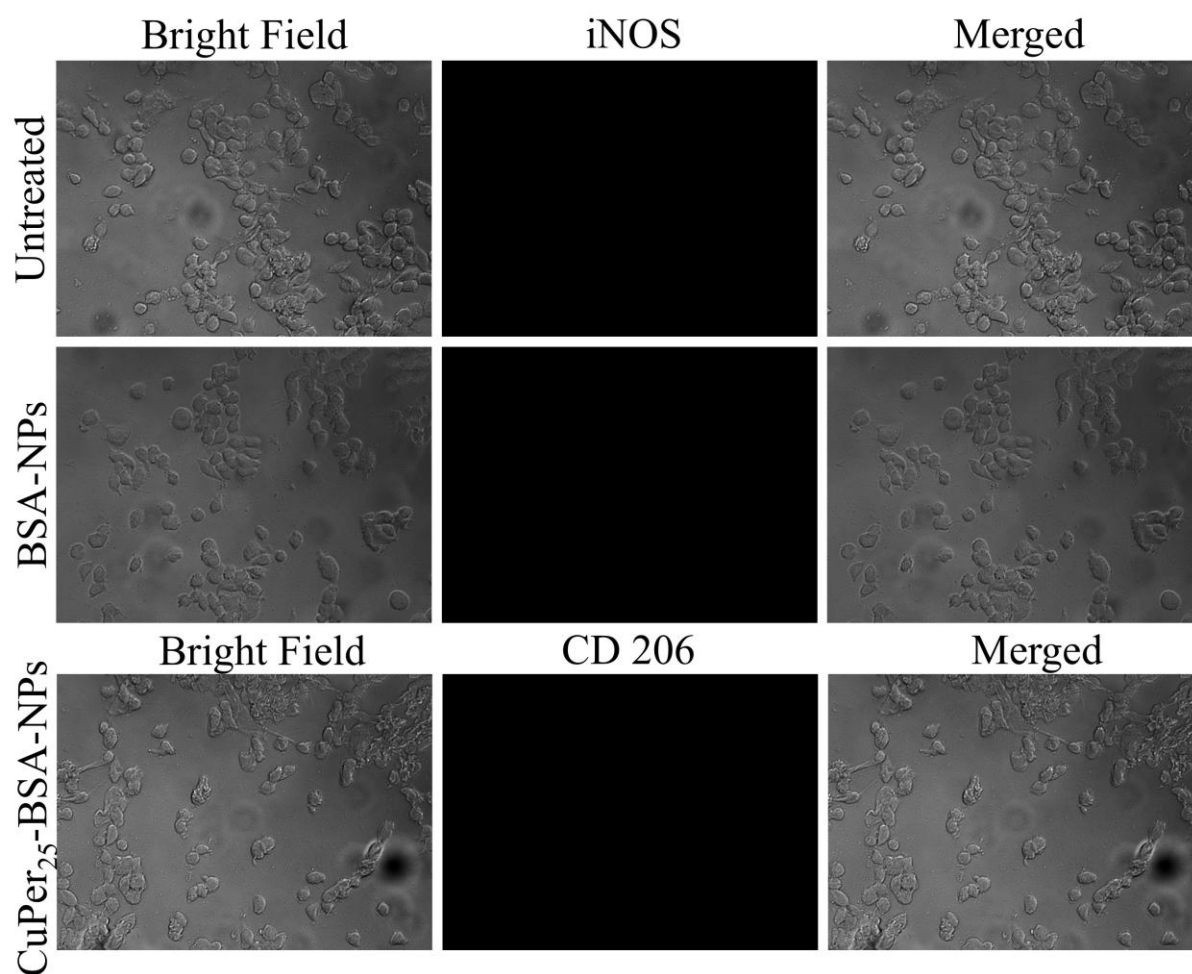
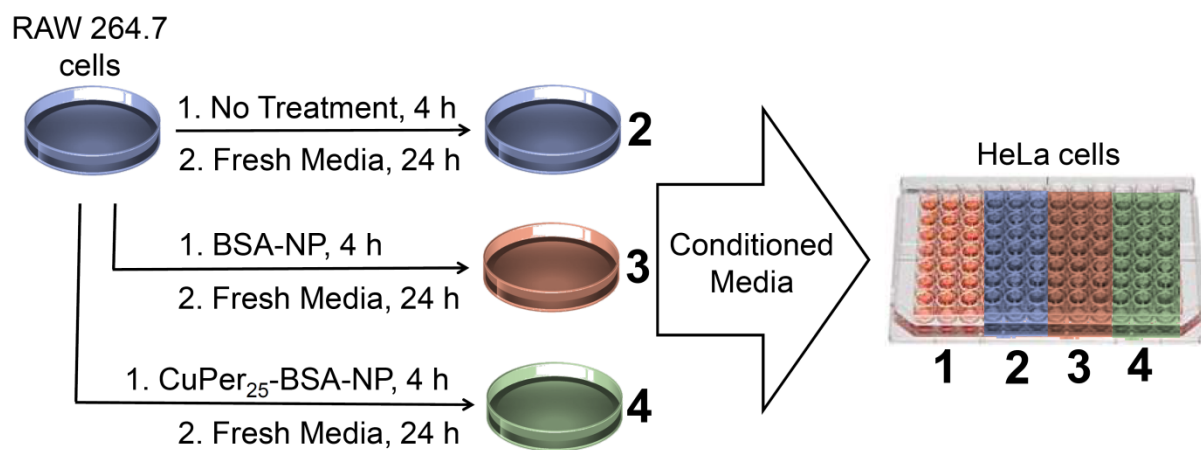


**Figure S19.** Top two rows respectively show fluorescence microscopy images of untreated and BSA-NP treated RAW 264.7 cells exhibiting no significant expression of iNOS. Bottom row shows fluorescence microscopy images of CuPer<sub>25</sub>-BSA-NPs treated RAW 264.7 cells exhibiting no significant expression of CD206.



**Scheme S2.** Scheme of the experiment performed to determine the toxicity of conditioned media obtained from RAW 264.7 cells under various conditions on HeLa cells. **1** represents the wells containing untreated HeLa cells.

## References:

- (1) Bump, E. A.; Reed, D. J. *In Vitro* **1977**, *13*, 115.
- (2) Park, E.-J.; Park, K. *Toxicology Letters* **2009**, *184*, 18.
- (3) Pal, R.; Chakraborty, B.; Nath, A.; Singh, L. M.; Ali, M.; Rahman, D. S.; Ghosh, S. K.; Basu, A.; Bhattacharya, S.; Baral, R.; Sengupta, M. *International Immunopharmacology* **2016**, *38*, 332.
- (4) Lunov, O.; Syrovets, T.; Loos, C.; Nienhaus, G. U.; Mailänder, V.; Landfester, K.; Rouis, M.; Simmet, T. *ACS Nano* **2011**, *5*, 9648.
- (5) Scherbart, A. M.; Langer, J.; Bushmelev, A.; van Berlo, D.; Habertzettl, P.; van Schooten, F.-J.; Schmidt, A. M.; Rose, C. R.; Schins, R. P. F.; Albrecht, C. *Particle and Fibre Toxicology* **2011**, *8*, 31.
- (6) Kumar, S.; Meena, R.; Paulraj, R. *Applied Biochemistry and Biotechnology* **2016**, *180*, 1257.
- (7) Ma, J. Y.; Zhao, H.; Mercer, R. R.; Barger, M.; Rao, M.; Meighan, T.; Schwegler-Berry, D.; Castranova, V.; Ma, J. K. *Nanotoxicology* **2011**, *5*, 312.
- (8) Wang, J.; Lee, J. S.; Kim, D.; Zhu, L. *ACS Applied Materials & Interfaces* **2017**, *9*, 39971.
- (9) Rojas, J. M.; Sanz-Ortega, L.; Mulens-Arias, V.; Gutiérrez, L.; Pérez-Yagüe, S.; Barber, D. F. *Nanomedicine: Nanotechnology, Biology and Medicine* **2016**, *12*, 1127.
- (10) Mulens-Arias, V.; Rojas, J. M.; Pérez-Yagüe, S.; Morales, M. P.; Barber, D. F. *Biomaterials* **2015**, *52*, 494.
- (11) Zanganeh, S.; Hutter, G.; Spitler, R.; Lenkov, O.; Mahmoudi, M.; Shaw, A.; Pajarinen, J. S.; Nejadnik, H.; Goodman, S.; Moseley, M.; Coussens, L. M.; Daldrup-Link, H. E. *Nature Nanotechnology* **2016**, *11*, 986.
- (12) Laskar, A.; Eilertsen, J.; Li, W.; Yuan, X.-M. *Biochemical and Biophysical Research Communications* **2013**, *441*, 737.
- (13) Wei, Y.; Wang, Z.; Yang, J.; Xu, R.; Deng, H.; Ma, S.; Fang, T.; Zhang, J.; Shen, Q. *Journal of Colloid and Interface Science* **2022**, *606*, 1950.
- (14) Xu, B.; Cui, Y.; Wang, W.; Li, S.; Lyu, C.; Wang, S.; Bao, W.; Wang, H.; Qin, M.; Liu, Z.; Wei, W.; Liu, H. *Advanced Materials* **2020**, *32*, 2003563.
- (15) Li, J.; Fan, J.; Gao, Y.; Huang, S.; Huang, D.; Li, J.; Wang, X.; Santos, H. A.; Shen, P.; Xia, B. *ACS Nano* **2023**, *17*, 1036.
- (16) Zhang, X.; Li, G.; Yin, J.; Pan, W.; Li, Y.; Li, N.; Tang, B. *Nano Letters* **2024**, *24*, 9104.
- (17) Cheng, J.; Zhang, Q.; Fan, S.; Zhang, A.; Liu, B.; Hong, Y.; Guo, J.; Cui, D.; Song, J. *Nanoscale* **2019**, *11*, 22849.
- (18) Jin, R.; Liu, L.; Zhu, W.; Li, D.; Yang, L.; Duan, J.; Cai, Z.; Nie, Y.; Zhang, Y.; Gong, Q.; Song, B.; Wen, L.; Anderson, J. M.; Ai, H. *Biomaterials* **2019**, *203*, 23.
- (19) Yang, Y.; Tian, Q.; Wu, S.; Li, Y.; Yang, K.; Yan, Y.; Shang, L.; Li, A.; Zhang, L. *Biomaterials* **2021**, *271*, 120739.
- (20) Tao, X.; Wan, X.; Wu, D.; Song, E.; Song, Y. *Journal of Hazardous Materials* **2021**, *411*, 125134.
- (21) Zhang, X.; Wang, Z.; Liu, Q.; Hu, X.; Mei, J.; Xu, D.; Zhou, J.; Zhang, X.; Li, Q.; Chen, H.; Su, Z.; Zhu, W.; Zhu, C. *Nano Today* **2024**, *54*, 102092.
- (22) Xu, J.; Zheng, B.; Zhang, S.; Liao, X.; Tong, Q.; Wei, G.; Yu, S.; Chen, G.; Wu, A.; Gao, S.; Qian, Y.; Xiao, Z.; Lu, W. *Advanced Functional Materials* **2021**, *31*, 2008022.
- (23) Ge, Y.; Zhang, J.; Jin, K.; Ye, Z.; Wang, W.; Zhou, Z.; Ye, J. *Acta Biomaterialia* **2023**, *167*, 551.